Characterization of a Mixed Convection Cell Designed for Phase Transition Studies in Moist Air

Konstantin A. Niehaus[1,2(✉)], Andreas Westhoff[1], and Claus Wagner[1,2]

[1] German Aerospace Center (DLR), Institute of Aerodynamics and Flow Technology, Göttingen, Germany
Konstantin.Niehaus@dlr.de
[2] Institute of Thermodynamics and Fluid Mechanics, Technische Universität Ilmenau, Ilmenau, Germany

Abstract. A detailed description of an experimental set-up designed for upcoming investigations of latent and sensible heat transfer in a cuboid sample with air in- and outlets is given. The container is heated at the rear and cooled at the transparent front wall. Temperature measurements reveal that both sides exhibit a mean temperature deviation below 2% relative to the temperature difference between the mean plate temperature and the ambient temperature. This is a suitable temperature distribution for such measurements. Tomographic particle image velocimetry covering the entire volume of the mixed convection cell exhibits a large-scale circulation due to forced convection with a buoyancy-induced flow close to the temperature controlled surfaces. Forced convection origins from a flow between the inlet and the outlet channel with a mean deviation of 1% from the mean velocity and a maximum absolute deviation of 0.04 m/s. Measurements were performed for Reynolds numbers ranging from $300 < \mathrm{Re} < 2000$ and Grashof numbers $\mathrm{Gr} < 1.2 \times 10^8$. A representative flow field obtained at $\mathrm{Re} = 620$ and $\mathrm{Gr} = 1.1 \times 10^8$ is presented as an example.

1 Introduction

The heat transfer in mixed convective air flows with phase transition is a phenomenon which occurs in nature and a plethora of technical applications. Condensate forming droplets leads to an increased heat transfer rate in comparison with film-wise condensation and therefore is advantageous in heat exchangers [13]. In contrast, condensation has negative effects in many other applications. For instance, fogging on the windshield or headlights of motor vehicles leads to restrictions when driving and a reduction of optical transparency influences road safety. In addition, a considerable amount of thermal energy is required for defogging, which leads to a range reduction when it comes to electric driving [16]. The design and modification of these components in terms of optimizing dehumidification or preventing misting is often based on experience and intuition [11]. Despite the enormous progress in numerical methods in recent years, there is still

© The Author(s), under exclusive license to Springer Nature Switzerland AG 2021
A. Dillmann et al. (Eds.): STAB/DGLR Symposium 2020, NNFM 151, pp. 483–493, 2021.
https://doi.org/10.1007/978-3-030-79561-0_46

a lack of reliable and applicable models for the numerical simulation of condensation in general, and in particular of droplet condensation on surfaces [10]. Due to the complexity of the physical processes that determine the heat transport and consequently the fogging on surfaces, reliable simulations are expensive and time-consuming, and therefore not suitable for industrial applications. Thus, the overall goal of this study is to develop a model, which allows the prediction of the condensation behavior on surfaces. In such a configuration the mass transport of vapor due to phase transition, the resulting latent and the sensible heat transfer are determined by the physical processes of convection, diffusion, the boundary conditions and the material properties of the surfaces. In a configuration where phase transition occurs, even smallest changes in the boundary conditions lead to significant changes in the vapor mass transfer. A major challenge of this study is the design and construction of an experimental set-up with the appropriate measurement technology. The focus lies on the characterization of the boundary conditions to ensure reproducibility for future experiments at high measurement accuracies.

In the present paper we introduce our set-up in detail and discuss the results of the flow and temperature characterization. The long-term goal is to control the effects of thermal and forced convection independently to map all physical processes that determine the fogging of headlamp windshields. In principle, the set-up represents a generic replica of a vehicle headlamp. The air flow inside automotive headlights is the result of the superposition of forced and thermal convection. In this case, the forced convection is characterized by the Reynolds number $Re = {}^{Ul}/_{\nu}$ and originates from ventilation holes at the rear wall of the mixed convection cell. In contrast thermal convection is the result of the heat emission from the internal light sources on the headlight's back and is characterized by the Grashof number $Gr = {}^{l^3 g \Delta T \beta}/_{\nu^2}$. Here, β, g and ν are the thermal expansion coefficient, gravitational acceleration and the kinematic viscosity of the working fluid air as a function of temperature and humidity. The experimental set-up consists of a rectangular cavity that is isothermally heated at the rear and cooled at the front. To compensate for pressure changes caused by temperature fluctuations, car headlights are designed as open systems to exchange air with the engine compartment through air inlets and outlets. The set-up simulates this using two venting channels. For the present configuration the characteristic velocity U is equal to the mean inlet velocity and l is a characteristic system length, which is the cell height in Gr and the inlet channel height for Re. Further, $\Delta T = \langle T_h \rangle - \langle T_c \rangle$ is the temperature difference between the mean temperature of a heating and a cooling plate. If T_c falls below the dew point T_{dp}, vapor mass flow $\dot{M}_v$ occurs due to phase transition. Fogging of surfaces thus depends on the flow velocity U, the air temperature T_{in}, the surface temperature T_c, the heat emission of the lamps $\dot{Q}_l$ as well as on the temperature of the light source T_h and the dew point temperature T_{dp}. We designed an experimental set-up which controls these parameters with high accuracy.

One of the first experimental studies on the issue of condensation inside automotive headlights was published by Hoines and Jiao in 1998 [2]. They studied the influence of the inlet positions on condensation and internal vapor density

distribution. Subsequently, numerical and experimental studies on fogging in consumer headlights by Siozawa et al. [14], Liu et al. [9] and Kim et al. [5] reveal a typical temperature difference between front lense and light source of $\mathcal{O}(10\,\mathrm{K})$ for semiconducting light sources and $\mathcal{O}(10^2\,\mathrm{K})$ for incandescent bulbs. Additionally, Kim et al. [5] studied the flow by means of stereoscopic particle image velocimetry (PIV). Their observed maximum velocities of $\mathcal{O}(10^{-1}\,\mathrm{m/s})$ match the results of Guzej and Zachar [1] and Zenin [17]. Further, Kim et al. [5] revealed three-dimensional flow structures and mixed convection. A set-up similar to the set-up presented in this paper was realized by Langebach [8, p. 35], who investigated the heat transport towards the light source to study the influence of venting positions and a sample geometry on bulb temperature. When comparing studies on this topic, it is evident that there is no canonical choice for the length scale within a headlight. So far, the following options for the lenght scale exist: path length of the flow between the vents, the devices width or height (i.e. Guzej [1]) or the inlet width (i.e. Langebach [8]). This results in maximum Reynolds numbers of $\mathcal{O}(10^5)$ and maximum Grashof numbers of $\mathcal{O}(10^9)$. Langebach [8] reported Reynolds numbers of $10^3 - 10^4$ and Grashof numbers of $\mathcal{O}(10^6)$ using the inlet width. Guzej et al. [1] investigated a case with $Re = 9.3 \times 10^3$ using the cell height in combination with the mean velocity above the front wall ($\mathcal{O}(10^{-2}\,\mathrm{m/s})$). In this work we employ the definition by Langebach [8].

2 Experimental Set-Up

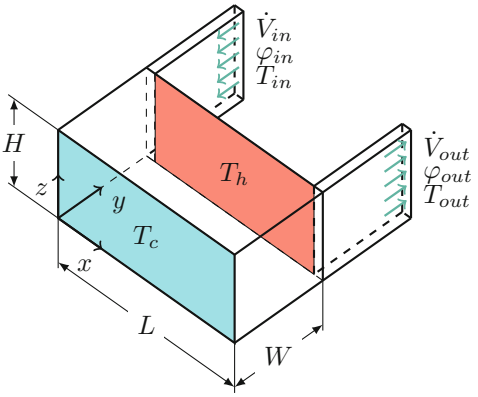

Fig. 1. Schematic set-up of the condensation cell: The cooling plate is colored blue (temperature T_c) and the heating plate is colored red (temperature T_h). Inlet and outlet conditions are characterized by means of humidity φ, temperature T_{in} and volume flow $\dot{V}$.

The set-up consists of a cuboid container with air in- and outlets. The aspect ratios of the cavity are $\Gamma_{yz} = {}^{W}/_{H} = 1$ and $\Gamma_{xz} = {}^{L}/_{H} = 2$, where $L = 500\,\mathrm{mm}$ denotes the length and $H = 250\,\mathrm{mm}$ the height of the sample which is equal to

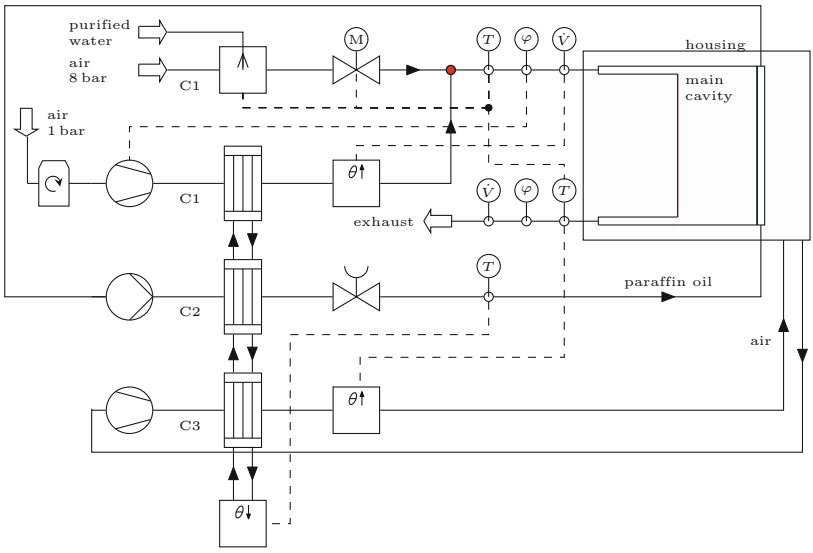

Fig. 2. Three control circuits for inlet temperature, humidity and volume flow of the inlet (C1), the cooling plate temperature (C2) and the ambient temperature of the condensation cell (C3). T, φ and $\dot{V}$ indicate temperature, humidity or volume flow measurements, respectively. A red dot marks the junction of humidifier and the volume flow section of C1.

its width W. Figure 1 depicts a schematic sketch of the sample. Forced convection originates from an inlet on the left and an outlet on the right side of the sample. Both extend over the entire cell height and are $w = 25\,\mathrm{mm}$ wide. The flow direction is indicated by turquoise arrows in Fig. 1. The red-colored area represents a 10 mm copper plate located between the vents with an electrical heating mat mounted on the back. The heating device extends over the entire cell height and has a length of 430 mm. 10 mm polyvinyl chloride is used as an insulation between the vents and the heating plate. To provide a homogeneous temperature distribution, the heating plate is covered by 60 mm styrodur with a thermal conductivity of $\lambda_D = 0.034\,\mathrm{W/m\,K}$. Fifteen resistance temperature devices (RTD) with an accuracy of approximately 0.1 K are distributed evenly over the entire heat plate. They are used to measure the mean temperature $\langle T_h \rangle$ and the spatial temperature distribution T_h. The probes are mounted in holes of 3 mm depth filled with a heat-conducting paste. The blue area in Fig. 1 indicates the condensing surface, which is composed of two parallel, 6 mm thick glass plates with a 20 mm gap. In between flows a countercurrent with respect to the air flow direction of paraffin oil at temperature $\langle T_c \rangle$. With the objective to obtain isothermal boundary conditions on the cooled surface, the device is equipped with eight volume-flow-controlled openings equally distributed over the height on both sides with a mixing section mounted in front of the inlets. All other walls of the sample are made of 10 mm thick glass plates. The sample itself

is placed in an air-filled, temperature controlled cuboid box a with height of 1 m, a length of 1.2 m and a width of 1 m. The ambient temperature T_∞ in the box is set to the mean sample temperature $(\langle T_{\text{in}}\rangle - \langle T_{\text{out}}\rangle)/2$ to obtain adiabatic boundary conditions. Furthermore, the configuration provides optical accessibility for the measurement of velocity fields.

Two flow meters are used to record the volume flow $\dot{V}$ at the in- and outlet of the sample with an accuracy of $\sigma_{\dot{V}} = 1.5\dot{V} + 0.05\,\text{l/min}$. The mean inlet velocity $\langle U\rangle$ is calculated using $\dot{V}/A$ with A being the inlet cross section. Before entering the cell, air passes a diffuser similar to the one studied by Köthe et al. [6] and an array of stainless steel meshes with size-to-wire thickness ratios of 311 µm/112 µm, 165 µm/80 µm and 95 µm/46 µm. These are followed by a honey comb flow straightener positioned 10 cm downstream of the inlet opening with a cell width of 3.2 mm and a wall thickness of 25 µm. The temperature of the air entering or leaving the sample is measured using eight RTD probes with an accuracy of 30 mK. The probes are evenly distributed over the cell's height. Figure 2 shows an overview of the set-up used to control the boundary conditions. The scheme is divided into three control cycles: C1 to C3. The cavity is shown on the top right inside the temperature-controlled housing. Before air enters (indexed with in) or leaves the cell (indexed with out), the vents' volume flow, mean temperature and mean humidity $\langle\varphi\rangle$ are measured in control cycle C1. The volume flow is generated by a radial fan. Additionally, the air system is equipped with an air dryer. Since the amplitude of the sensor noise scales with its absolute value, τ depends on the Reynolds number and is chosen such that the standard error of the mean is below 4 l/min. This is equivalent to a mean velocity deviation of 0.01 m/s. A circulation chiller with a 5 kW cooling output at 20 °C is used to set the front plate temperature. 16 RTDs with an approximate accuracy of 0.1 K are used to measure the mean cooling plate temperature.

Fig. 3. Photograph of the housing with a low momentum ceiling ventilation (white) and the test section inside with the transparent cooling plate and its tubing.

The chiller is used to set T_c, which is the lowest temperature in the system. Consequently, C1 and C3 are equipped with electrical heaters to set T_{in} and T_∞ independently. The dry and temperature-controlled air mixes with humidified air at the joint indicated with a red dot.

Since the results presented here are obtained in a dry environment with no phase transitions, further details on the control accuracies and measurement uncertainties of the humidification system will be given in a consecutive work. Inside the housing, the temperature is measured using RTDs in combination with SHT85 sensors. Figure 3 provides an overview of the housing with the test section inside. The housing is equipped with a low-momentum ceiling ventilation system in order to provide a homogeneous spatial temperature distribution at a low flow velocity. The black box

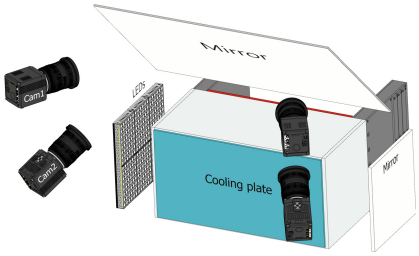

Fig. 4. Tomographic PIV set-up: Four cameras imaging the cell via a mirror mounted above the cell. A LED array illuminates the cell from the left side. The light is reflected back into the cell via a second mirror on the right.

between the set-up's supports is filled with approx 0.7 t of sand to minimize vibrations. Tomographic PIV is used to determine the internal velocity distribution $U(\mathbf{x})$. The PIV measurement set-up is depicted in Fig. 4. Four cameras imaging the main cavity via a surface mirror mounted on top of the cell. LEDs are mounted on the left wall close to the inlet section. Seeding particles are introduced close to the opening of the inlet channel. The measurement volume covers the entire cell. It is lit using two multi-LED illuminators positioned at a distance of 15 cm from the sidewall. On the opposite side, a mirror is mounted to increase the light intensity in the measurement volume. For a detailed description of the light source, see Stasicki et al. [15]. As seeding particles, buoyancy-neutral helium-filled soap bubbles (HFSB) are injected into the flow at the beginning of the inlet to provide a homogeneous particle distribution at the sample inlet. The mean diameter of the HFSB is 0.3 mm.

By injecting the HFSB, an additional volume flow of maximum $\dot{V}/10$ is generated. However, the total volume flow remains constant. The time series of images are recorded by four PCO Edge 5.5 (double shutter) in Scheimpflug condition together with $f = 21$ mm (Distagon T* 2.8, Carl Zeiss), whose aperture is set to $f/11$. Volumetric self-calibration, reconstruction and correlations are obtained using an in-house code that is described in detail in Kühn et al. [7]. The final interrogation volume used for the cross-correlation step in the multigrid process includes $32 \times 32 \times 32$ voxels with a 50% overlap. To characterize the internal convective flow, a wide parameter range is studied. The overview of the parameter combination of forced (Re) and thermal convection (Gr) is given in Fig. 5. The graphic depicts the set of tuples (Gr and Re), with bars indicating 1σ-uncertainties.

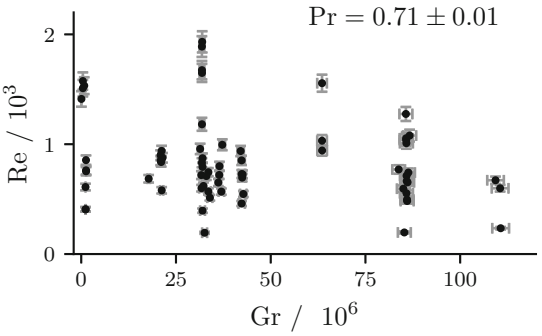

Fig. 5. Parameter space covered in the PIV measurement campaign. A dot indicates a measurement run with corresponding parameters with bars indicating the uncertainty.

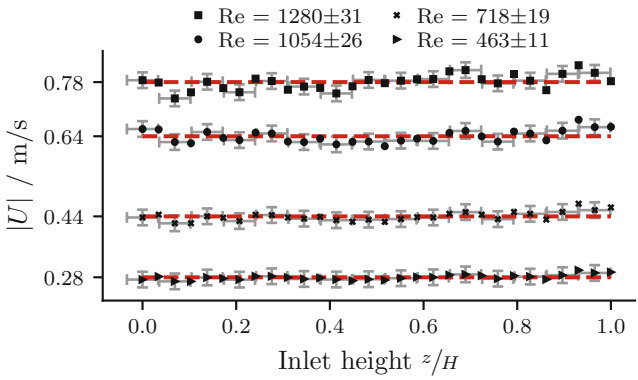

Fig. 6. Inlet velocity profile ($x = 12.5\,\text{mm}$) of the inlet channel in z-direction for different Re with characteristic length $w = 25\,\text{mm}$. Dashed red lines indicate the average velocity.

3 Results

At $x = 12.5\,\text{mm}$ the vertical inlet velocity distribution was measured using an omnidirectional draught probe with an uncertainty of $\pm(0.02\,U + 0.02\,\text{m/s})$. The probe was positioned at 30 sites along the inlet height. The measurement duration was 10 s with a sampling frequency of 10 Hz. Figure 6 shows the time-averaged velocities and the above defined uncertainties as a function of Re. Uncertainties of the mean are displayed only for every other value for the sake of visibility.

The numbers along the y-axis and the dashed line presents the mean velocities. For all Re and measurement positions the relative deviation from the mean lies below 1% i.e. below 0.04 m/s. This is below the deviations of 4% reported by Kühn [4, p. 88], who investigated forced and mixed convection by means of tomographic PIV. In addition, the homogeneity of the temperature distribution

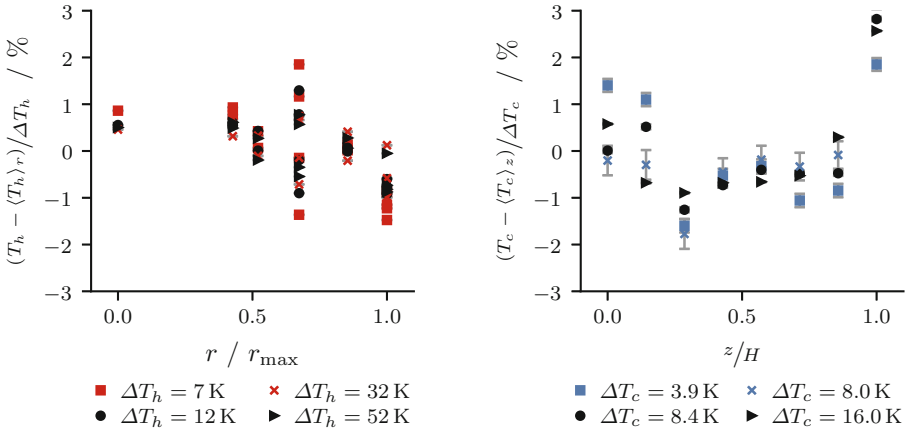

(a) Temperature deviation $T_h - \langle T_h \rangle_r$ normalized by the temperature difference $\Delta T_h = |\langle T_h \rangle_r - T_\infty|$ in percent as a function of the distance r from sensor to plate center for different ΔT_h.

(b) Temperature deviation $T_c - \langle T_c \rangle_z$ normalized by the temperature difference $\Delta T_c = |\langle T_c \rangle_h - T_\infty|$ in percent as a function of the heigth for different ΔT_c.

Fig. 7. Temperature distributions for heating and cooling plate measured using RTD temperature probes at various mean surface temperatures.

of the heating plate was measured. Figure 7a shows the spatial temperature distribution of the heating plate, with the radial distance from the sensor position to the plate center normalized with $r_{\max} = 280\,\mathrm{mm}$ on the ordinate. Different markers correspond to varying temperature differences ΔT_h. The measurement case with the smallest temperature difference shows the highest relative temperature deviations. The radial distribution of deviations from the mean heating plate temperature (Fig. 7a) exhibits a maximum relative deviation below 2% everywhere. The maximum of the absolute deviation occurs at $\Delta T_h = 16\,\mathrm{K}$ with a temperature difference of 0.4 K for $|T_\infty - \langle T \rangle_{t,z}|$. This deviation is of the same magnitude as the uncertainties reported by Schmeling et al. [12] ($\Delta T = 21.2\,\mathrm{K}$, $\sigma = 2.2\%$). The distribution of temperatures inside the cooling plate is shown in Fig. 7b. Measurements were conducted for various temperature differences $\Delta T_c = |T_\infty - \langle T_c \rangle_z|$ between the mean housing temperature and the mean cooling plate temperature. This difference represents the normalized temperature variations over the height of the cooling plate. The temperature distribution in Fig. 7b exhibits relative values similar to those of the heating plate, while the maximum absolute deviation is 0.4 K at a temperature difference of 16 K with a relative deviation of 2.6% at $z = H$. This may be caused by an air cavity in the vicinity of the sensor, the missing insulation during the measurement or a malconfigured volume flow in this area and will be adjusted in future measurements. The deviations are still below those reported by Kästner et al. [3] who also employed a transparent temperature-controlled surface (heated) in a convection

experiment. At a temperature difference of 16 K they report a mean deviation of 1.7%, whereas the deviation for the set-up in this study is 0.7%. Moreover, except the value at $z = H$, all deviations are smaller than those reported by Schmeling et al. [12].

In addition to the inflow and boundary conditions, the resulting flow patterns in the sample are of utmost importance since the structures have a strong impact on the heat and thus, on the vapor mass transfer. Examples of mean velocity fields plane through the cell center parallel to the xy-plane and the yz-plane are given in Fig. 8 with $\mathrm{Gr} = 1.1 \times 10^8$ and $\mathrm{Re} = 620$. The in-plane flow is indicated by vectors, while the out-of-plane component is color-coded. The time-averaged vector fields are calculated by means of 630 instantaneous vector fields with a recording frequency of 25 Hz. Due to reflections areas close to in- and the outlet are masked. The flow originates at the inlet $(x, y) = (0, W)$ and is directed towards the cooling plate. At the front wall the flow is redirected parallel to it and detaches at $x/L = 7/8$. Between the cooling plate and the outlet the flow separates into one part leaving the cell through the outlet and another part returning to the inlet parallel to the heating plate. The center line of this large scale circulation can be seen in yz-plane on the left of Fig. 8 with $u = 0$. It clearly shows an asymmetric shape along the z-axis and the 3D flow structure. The presence of thermal convection can be seen in both velocity fields and is indicated by $u_z < 0$ close to the cooling plate and $u_z > 0$ at the heating plate. The influence of Gr and Re has to be characterized in an in-depth analysis of all measurement cases summarized in Fig. 5. However, the present mean velocity fields give a general understanding of the flow structure and demonstrate, that a tomographic PIV measurement of the entire cell has been implemented successfully.

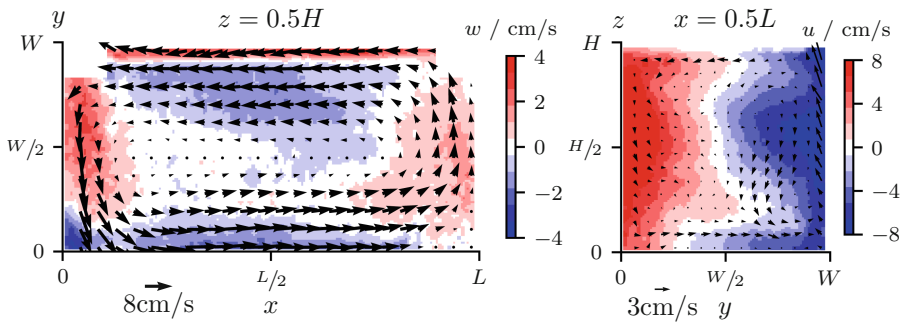

Fig. 8. Time-averaged (26 s, 630 frames) velocity field at $z = 0.5H$ parallel to the xy-plane (left) and at $x = 0.5L$ parallel to the yz-plane (right) with $\mathrm{Re} = 620$ and $\mathrm{Gr} = 1.1 \times 10^8$. Vectors indicate the in-plane and colors the out-of-plane flow.

4 Conclusion

In the present paper we give a detailed description of an experimental set-up designed to investigate latent and sensible heat transfer in a cuboid sample with air in- and outlets. The container is heated at the rear and cooled at the front. Both sides exhibit a measured mean temperature deviation below 2% relative to the temperature difference between the mean plate temperature and the ambient temperature. Forced convection origins from a flow between an inlet and an outlet channel. The homogeneity of the inlet velocity profile is measured at different Reynolds numbers with a mean deviation of 1% from the mean velocity and a maximum absolute deviation of 0.04 m/s. Measurements were performed for Reynolds numbers ranging from $300 < \mathrm{Re} < 2000$ and Grashof numbers $\mathrm{Gr} < 1.2 \times 10^8$. The accuracies of the boundary conditions are compared to other experiments focusing on the investigation of convective air flows. The goal to achieve boundary conditions with uncertainties equal to or below those of experiments investigating similar flow conditions is reached. Hence, the set-up is suited for reproducible measurement campaigns. Furthermore, the optical accessibility allows for tomographic PIV or particle tracking velocimetry measurements covering the entire sample. A first result of this campaign exhibits a large-scale circulation due to forced convection with a buoyancy- induced flow close to the temperature controlled surfaces.

Acknowledgment. The authors like to thank Annika Köhne for proof-reading this work.

References

1. Guzej, M., Zachar, M.: CFD simulation of defogging effectivity in automotive headlamp. Energies **12**(13), 2609 (2019)
2. Hoines, L., Jiao, J.: Environment leading to condensation in automotive lamps. SAE Trans. 682–685 (1998)
3. Kästner, C., Resagk, C., Westphalen, J., Junghähnel, M., Cierpka, C., Schumacher, J.: Assessment of horizontal velocity fields in square thermal convection cells with large aspect ratio. Exp. Fluids **59**(11), 1–13 (2018)
4. Kühn, M.: Untersuchung großskaliger Strömungsstrukturen in erzwungener und gemischter Konvektion mit der tomografischen Particle Image Velocimetry. PhD thesis, TU Ilmenau, August 2011
5. Kim, D., et al.: Velocity field measurement on natural convection inside an automotive headlamp using time-resolved stereoscopic particle image velocimetry. Int. J. Heat Fluid Flow **77**, 19–30 (2019)
6. Köthe, T., Herzog, S., Wagner, C.: Shape optimization of aircraft cabin ventilation components using adjoint CFD. In: Engineering Optimization 2014, pp. 675–680. CRC Press, September 2014
7. Kühn, M., Ehrenfried, K., Bosbach, J., Wagner, C.: Large-scale tomographic PIV in forced and mixed convection using a parallel SMART version. Exp. Fluids **53**, 91–103 (2012)
8. Langebach, J.: Beiträge zur thermischen Auslegung von Automobilscheinwerfern. Univ.-Verlag Ilmenau (2008)

9. Liu, H., Jiang, L.F., Hu, C.G., Chen, X.L., Lin, J.D.: Method of lamp fogging discrimination. In: Applied Mechanics and Materials, vol. 248, pp. 179–184. Trans Tech Publications (2013)
10. Oxyzoglou, I., Tejero, A.: Prediction of condensation forming in automotive headlights using CFD. Technical report, University of Thessaly (2018)
11. Poorman, T., Bielecki, J., Chang, M., Belsare, S., El-Khatib, F.: Automotive lighting thermal performance prediction methods. In: SAE Technical Paper Series. SAE International (2001)
12. Schmeling, D., Bosbach, J., Wagner, C.: Simultaneous measurement of temperature and velocity fields in convective air flows. Meas. Sci. Technol. **25**(3), 035302 (2014)
13. Schmidt, E., Schurig, W., Sellschopp, W.: Versuche über die Kondensation von Wasserdampf in Film- und Tropfenform. Forsch. Ingenieurwes. **1**, 53–63 (1930)
14. Shiozawa, T., et al.: Thermal air flow analysis of an automotive headlamp: the PIV measurement and the CFD calculation for a mass production model. JSAE Rev. **22**(2), 245–252 (2001)
15. Stasicki, B., Schröder, A., Boden, F., Ludwikowski, K.: High-power LED light sources for optical measurement systems operated in continuous and overdriven pulsed modes. In: Lehmann, P., Osten, W., Gonçalves, A.A. (eds.) Optical Measurement Systems for Industrial Inspection X. SPIE, June 2017
16. Westhoff, A.: Experimentelle Untersuchung des Einflusses der O-ber-fläch-en-beschaf-fen-heit von Scheiben auf die Kondensatbildung. Technical report, FAT, December 2017
17. Zenin, S.: Numerische und experimentelle Untersuchungen zum Wärmetransport in einem Automobilscheinwerfer. Univ.-Verlag Ilmenau (2007)